A Versatile Nb₂O₅/SnO₂ Heterostructure for Different Environmental Purposes: Water Treatment and Artificial Photosynthesis

Thaís Aparecida Rodrigues, [b] Paulo Henrique Eleutério Falsseti, [c] Douglas Mendes da Silva Del Duque, [a] Gelson T. S. T. da Silva, [d] Osmando Ferreira Lopes, [e], [f] Waldir Avansi Junior, [c] Caue Ribeiro [d] and Vagner Romito de Mendonça*[a], [b]

Abstract

A versatile Nb₂O₅/SnO₂ heterostructure, adequate for different processes, was successfully synthesized by adding SnO2 to the hydrothermal Nb₂O₅ synthesis process. The presence of SnO₂ dispersed over Nb₂O₅ did not modify its crystalline structure. On the other hand, the properties of the material were strongly affected by coupling the semiconductors. The heterostructure exhibited enhanced photocatalytic performance compared to pure Nb₂O₅ in the degradation of rhodamine B dye and the amiloride medication under UV radiation, as well as during CO2 photoreduction. Moreover, the heterostructured material was more efficient at removing the cationic species methylene blue dye and Mn (II) from the aqueous solution through adsorption than pure Nb2O5. Its versatility has been explained by reference to the negative surface charge induced by SnO2 and the charge separation in the heterostructure, which increases their lifetimes, making it possible to reach the surface of the material and promote the reaction in the oxidative and reductive processes. Our results indicate that coupled Nb₂O₅/SnO₂ can be a unique platform to different forms of environmental treatment.

Introduction

The population increase and economic growth of recent decades has triggered severe environmental problems. Amongst these is the contamination of water by dyes, pesticides, medicines and metals [1] from agricultural and industrial activities and the release of CO_2 into the atmosphere from the burning of fossil fuels. [2] Several technologies based on the application of different materials have been developed to mitigate these issues. [3–5] Examples include semiconductors,

such as TiO_2 and ZnO, which photooxidize organic compounds in aqueous systems;^[6,7] SiO_2 removes Mn(II) from effluents through adsorption;^[8] and CuO catalyzes CO_2 photoreduction processes.^[9]

However, semiconductors in isolated form exhibit some limitations, such as rapid electron/hole recombination and poor solar light harvesting. Thus, the development of composite materials appears to be a viable way to improve photocatalytic performance. The union of different compounds, with noncontinuous and multiphase microstructure, improves the properties for most diverse environmental systems.^[10]

Nb₂O₅ stands out amongst the candidate semiconductors for composites and has been applied in isolated form or coupled to other materials.[11-16] Lopes et al.[15] showed Nb₂O₅ application for Rhodamine B dye and atrazine pesticide degradation under UV radiation. Hydroxyl radicals mainly conducted the process, while under visible radiation, by the sensitization process. Wolski et al.[16] showed the influence of H₂O₂ on the efficiency of Rhodamine B photodegradation over Nb₂O₅. It was demonstrated that Nb₂O₅ can also be applied for dye removal in a Fenton-like process by adding hydrogen peroxide in dye solution. However, the materials efficiency could be dramatically enhanced by the UV radiation combining advanced oxidation and Fenton-like process due to the generation of highly oxidizing species. Lacerda et al.,[17] in turn, demonstrated the application of a composite formed by Bentonite clay and Nb₂O₅ to a textile dye's photodegradation under UV radiation. The application of clay composites makes possible the recovery and reuse of semiconductor material. Silva et al.[18] showed that Nb2O5 can also be applied in

[a] Prof. Dr. V. R. De Mendonça, D. M. S. D. Duque Federal Institute of Science, Education, and Technology of São Paulo Av. João Olímpio de Oliveira, 1561, Itapetininga/SP, CEP 18208-000, Brazil E-mail: vrm@ifsp.edu.br [b] Prof. Dr. V. R. De Mendonça, T. A. Rodrigues Federal University of São Carlos Rod. SP-264, km 110, Sorocaba/SP, CEP 18052-780, Brazil [c] P. H. E. Falsetti, Prof. Dr. W. Avansi Jr. Department of Physics Federal University of São Carlos Rod. Washington Luís, km 235, São Carlos/SP, CEP 13565-905, Brazil [d] Dr. G. T. S. T. Da Silva, C. Ribeiro Nanotechnology National Laboratory for Agriculture (LNNA), Embrapa Instrumentation Rua XV de Novembro, 1452, CEP 13561-260, São Carlos/SP, Brazil. [e] Dr. O. F. Lopes Laboratory of Photochemistry and Materials Science, Institute of Chemistry, Federal University of Uberlandia Av. João Naves de Ávila, 2121, CEP 38400-902, Uberlandia/MG, Brazil; [f] Dr. O. F. Lopes Institute of Energy and Climate Research (IEK-14): Electrochemical Process Engineering Forschungszentrum Jülich GmbH Zip Code 52425, Jülich, Germany.

reductive reactions, where the surface acidity of Nb_2O_5 has an important role in its selectivity during CO_2 photoreduction processes. The product ratio (CO or CH_4) depends on the initial surface acidity, which is a striking feature of this material. Moreover, Nb_2O_5 materials were shown to be able to remove cationic species from water via adsorption, as reported by Nakagomi^[19] with methylene blue adsorption. However, despite these various examples, pure Nb_2O_5 does not meet the performance criteria required for practical applications, and it is therefore necessary to develop composites to overcome some of its drawbacks.

Heterostructures consist of composites that present different band structures and yield new electronic properties.[20] Depending on the materials' band structure and work functions, there may be, after the materials' excitation, spatial separation of photogenerated negative electrons and positive holes. This heterostructure, called type II, is the most suitable for promoting oxi-reduction reactions. It increases the photogenerated charges' lifetime, which is an important factor in the photochemical efficiency of semiconductors.[20-22] Several heterostructures have been applied to photocatalytic processes, such as Nb₂O₅-TiO₂, [23,24] SnO₂-TiO₂, [25,26] g-C₃N₄- Nb_2O_5 , [27,28] CeO_2 - Nb_2O_5 , [29] SnO_2 -ZnO[30] and SnO_2 - MoS_2 . [31,32] SnO₂ has a suitable band structure for assembly with Nb₂O₅ in a type-II heterostructure, [32] but has been scarcely reported upon. Moreover, as the heterostructures imply a different phase distribution of the semiconductor' surface, these materials have different surface characteristics that interfere with its catalytic properties - the surface charge (often neglected) affects the adsorption of some species.[33]

Thus, this work aims to obtain the Nb₂O₅/SnO₂ heterostructure by means of the hydrothermal method and evaluate its applications in different environmental remediation processes, i.e., adsorption and heterogeneous photocatalysis in both oxidative (organic pollutant degradation) and the reduction process (CO₂ photoreduction). Our results depict a panorama of this material's possible applications, demonstrating its versatility for environmental purposes.

Results and Discussion

Characterization

Figure 1 shows the X-ray diffraction patterns, as well as the Raman and FTIR spectra of the synthesized samples. The preformed SnO_2 nanoparticles were indexed to the cassiterite phase (JCPDS, n^o 41-1445), as expected (Figure 1(a)). $^{[33]}$ The diffraction peaks of the SnO_2 samples exhibited relatively broad half-height peaks, which can be attributed to the nanoparticles' small size. $^{[35]}$ The diffraction pattern of the Nb_2O_5 sample also shows widened peaks, and the indexed crystallographic plans refer to niobic acid (Nb_2O_5 . nH_2O – JCPDS, n^o 27-1003). This feature is associated with the high degree of hydroxylation for Nb_2O_5 , which resulted from the synthesis methods employed. $^{[15,33,34,36]}$

Thus, as expected, the XRD pattern of the synthesized Nb_2O_5/SnO_2 composite has the main peaks of Nb_2O_5 with an enlarged and defined profile; however, the widening peak at 26° can be observed compared to the same region of the pure Nb_2O_5 sample, suggesting a possible contribution of the SnO_2 (110) peak. Additionally, two new peaks between 30 and 35 °

highlighted with (*) in Fig. 1(a) can be observed in the composite XRD pattern. These two peaks are probably related to a Sn-Nb-O compound with a pyrochlore structure $(SnNb_2O_6)$, $^{[37]}$ indicating an interface between the materials. This lack of clarification about the presence of SnO_2 may be associated with crystallite size, overlapping peaks and the small amount of SnO_2 nanoparticles in the composite.

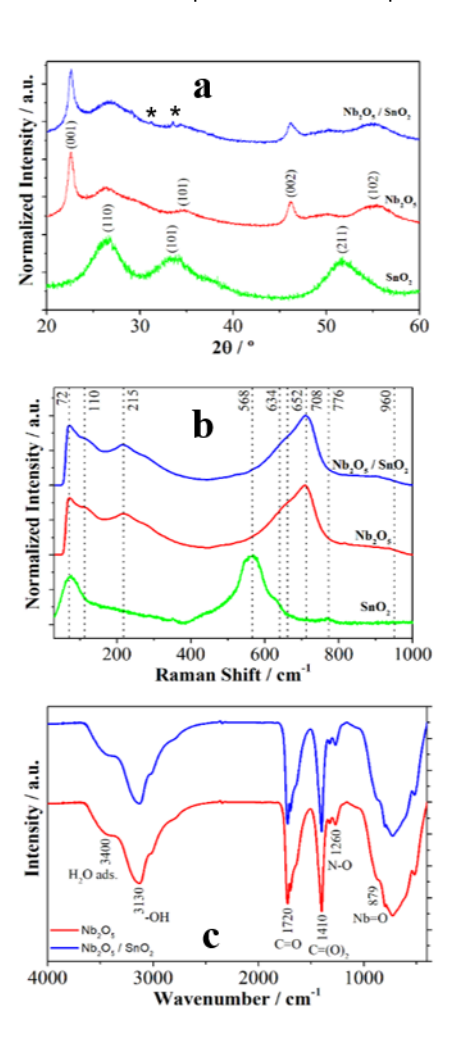


Figure 1. Structural and superficial characterization of the synthesized Nb_2O_5 and Nb_2O_5/SnO_2 heterostructures (a) XRD pattern; (b) Raman spectra; and (c) FTIR spectra.

Figure 1(b) displays the Raman spectra of the synthesized samples. The Raman spectrum of the Nb_2O_5 sample exhibits wide and intense peaks, a characteristic of this material. $^{[15,32]}$ These peaks are centered at 215 cm $^{-1}$, which can be attributed to the folding modes of O-Nb-O groups; at 652 and 708 cm $^{-1}$, it can be attributed to the asymmetric stretching of Nb-O groups in the distorted polyhedra of NbO $_6$, NbO $_7$, and NbO $_8$; and at 860 cm $^{-1}$, to the symmetrical stretching of NbO $_2$ groups and associated with the formation of di- η^2 -peroxo systems with cis-lateral geometry. The peaks at 568, 634, and 776 cm $^{-1}$ are characteristics of rutile SnO_2 . $^{[38]}$ The composite spectrum of Nb $_2O_5/SnO_2$ shows that the dominant dispersions can be attributed to Nb $_2O_5$, mainly due to the small SnO_2 . Once again, the SnO_2 did not change the Nb $_2O_5$ structure. $^{[17,43,44]}$

The Fourier transform infrared (FTIR) spectroscopic data from 4000 to 400 cm⁻¹ is presented in Figure 1(c). We performed this analysis to study the surface of the materials. As previously reported,^[33] some of the groups from the synthesis

environment remain in the resulting material as impurities. These groups, such as $C=(O)_2$, C=O, and N-O, may be responsible for stabilizing the Nb_2O_5 phase. Interestingly, they occur in both samples, showing that SnO_2 in the Nb_2O_5 synthesis environment did not modify its crystallization process.

Figure 2 includes TEM and SEM images of preformed SnO₂ nanoparticles used as a precursor, pure Nb2O5, and Nb₂O₅/SnO₂ heterostructures. Furthermore, it also shows the elemental mapping of the synthesized heterostructure. Figure 2(a) confirms that the preformed SnO₂ nanoparticles have a diameter of around 5 nm, as expected. Additionally, on the inset, the crystallographic plane is identified in relation to the rutile phase of SnO₂, following the XRD presented in Figure 1(a). The morphology of pure Nb₂O₅ is typical of the hydrothermal crystallization of Nb-peroxide complex, with an agglomeration of quasi-spherical nanoparticles with an approximate size of 30 nm (Figure 2(b)).[15] The synthesized Nb₂O₅/SnO₂ heterostructures in Figure 2(c) exhibits a surface primarily composed of quasi-spheres, which can be attributed to Nb₂O₅. However, the modification in the Nb₂O₅ texture is indicative of SnO₂ nanoparticles. The elemental mapping images for Nb₂O₅/SnO₂ heterostructures (in the same region of Figure 2(d)) shows Sn species, confirming that SnO₂ is evenly distributed in the composite (Nb and O have also been identified). Figure 2(e) displays a bright field STEM image and their corresponding HAADF (Fig. 2(f)) (high-angle annular dark-field) image for the heterostructured sample. HAADF images evidenced the two distinct nanostructures, with the presence of nanorods and very small nanoparticles presenting size around 5nm (some of them indicated by red arrows). The presence of nanorods could be attributed to Nb₂O₅, according to Lopes et al.[15] On the other hand, the very small bright spots could be attributed to SnO₂ nanoparticles, as observed in Fig. 2(a), specially due to difference in Z between Nb and Sn. In this way, this figure confirms the presence of small quantity of SnO₂ nanoparticles distributed on Nb₂O₅ structures. The intimate contacts between Nb2O5 and SnO2 suggest that the synthesized composite may have promising catalytic properties. The EDX spectrum of a heterostructure obtained in a mass proportion of 1:15 ($SnO_2:NH_4H_2[NbO(C_2O_4)_3].nH_2O$) is in Figure S1, confirming the small molar proportion between SnO₂ and Nb₂O₅. As SnO₂ nanoparticles are smaller than Nb₂O₅ particles, this low proportion would be enough to promote several points of contact, leaving the Nb₂O₅ surface free to promote the reactions, as SnO2 is not an active photocatalyst.[21]

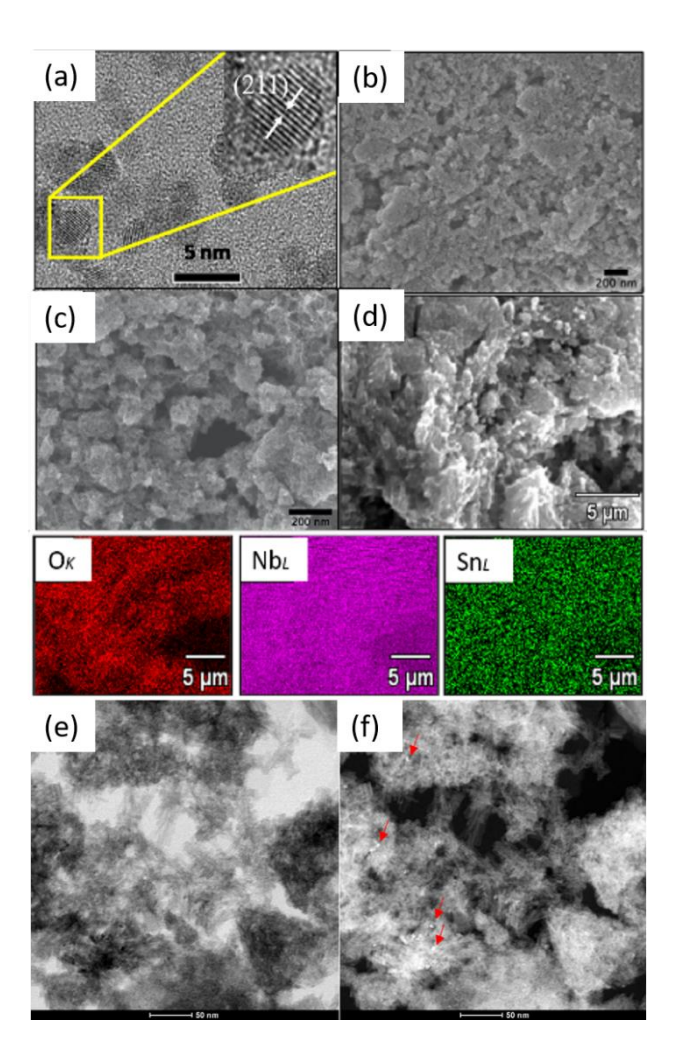


Figure 2. (a) HRTEM images of SnO_2 nanoparticles used in the heterostructures' synthesis; representative SEM images of the as-prepared (b) Nb_2O_5 ; (c) and (d) Nb_2O_5/SnO_2 heterostructures. Below the images is EDX elemental mapping of the Nb_2O_5/SnO_2 heterostructure sample (O, Nb and Sn) obtained from image (d); STEM images of Nb_2O_5/SnO_2 : (e) Bright field; (f) corresponding HAADF showing SnO_2 nanoparticles as bright spots (red arrows) in the Nb_2O_5 matrix.

The bandgap energies of the synthesized samples were determined by UV–vis diffuse reflectance spectroscopy and the results are exhibited in Figure 3. The Nb_2O_5 sample has a bandgap of around 3.2 eV, similar to that reported in the literature. The Nb_2O_5/SnO_2 heterostructure showed a small redshift on the absorption edge, widening the absorption spectrum and allowing the material to be activated with 3.1 eV. This is a significant result, as it reveals that coupling SnO_2 nanoparticles over Nb_2O_5 did not markedly change the bandgap of the material, indicating that there no doping process took place during the synthesis.

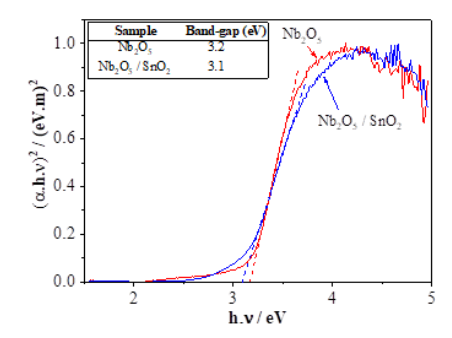


Figure 3. Plot of $(\alpha.h.n)^2$ against hv from the UV–vis diffuse reflectance for Nb₂O₅ and Nb₂O₅/SnO₂ samples. The bandgap values are described in the inset

Photocatalytic Performance of the Nb₂O₅/SnO₂ samples

The changes in the photocatalytic activity of the Nb2O5 materials induced by the presence of SnO₂ nanoparticles was explored primarily in the context of the degradation of different organic molecules, RhB dye and the Amiloride medication under UV radiation. Prior to the photocatalytic experiments, all of the samples were kept in contact with the organic molecules' solutions in darkness conditions for 30 min, until the reaction reached the adsorption/desorption equilibrium. This step is also important to check the occurrence of an acid catalyzed reaction, since Nb₂O₅ presents a high surface acidity. In the present case, since the samples differs only by the preformed SnO₂ nanoparticles in the synthesis environment, the surface acidity would not be different between them. In fact, the analysis of acid sites in the samples, measured by the ionicexchange procedure followed by titration of the acid species released in alkaline solution by the solid acid, as described by Silva et al.[18] showed a total acid sites concentration around 1.5 mmol.g-1 for both samples. Despite this value, it was observed that the pollutants concentration did not change during the time in darkness, indicating that the acid-catalyzed mechanism did not take place during the experiments.

Figure 4 presents the results for the RhB photodegradation essays. RhB dye was chosen due to its zwitterion nature in its natural pH, which makes the molecule less susceptible to adsorption on the negative charge surfaces.[41] As previously mentioned, the adsorption was negligible after 30 minutes of contact. As is shown in Figure 4 (a), Nb₂O₅/SnO₂ showed a higher RhB degradation rate than isolated materials. These results confirm that contact amongst the semiconductors is essential to increasing the material's photoactivity, probably due to the charge migration within the materials. The heterostructure synthesis was also performed using different mass proportions between SnO₂ $NH_4H_2[NbO(C_2O_4)_3].nH_2O$ (1:15 and 1:60), always retaining the same mass of Ammonium Niobium Oxalate in the reactor. samples exhibited lower capability RhB photodegradation (Figure S2), indicating that the heterostructure obtained using a proportion of 1:30 $(SnO_2:NH_4H_2[NbO(C_2O_4)_3].nH_2O)$ was able to promote a higher flux of charges across the semiconductor interface.

Considering the decay of the RhB dye concentration with a first order kinetic, the data can be linearized, as is shown in Figure 4(b). The slope of the curve reflects the degradation rate

constants k', depicted in the inset figure. The SnO₂ in the Nb₂O₅ increases the rate constant by about 145 %.

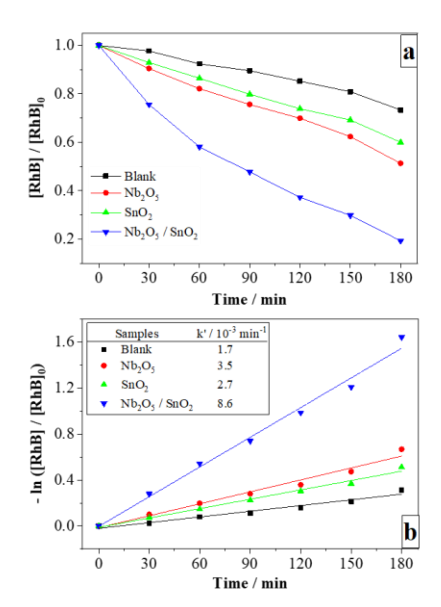


Figure 4. (a) Kinetic of photocatalytic degradation of RhB with synthesized samples; (b) First-order kinetic for the samples. On the inset, k values obtained by linear regression.

As the heterogeneous photocatalysis process depends on the active sites of the semiconductor's surface, the specific surface area (SSA) was determined and related to photocatalytic activity, as is shown in Table 1.

Table 1. SSA values and rate constant k`/SSA ratio of the heterostructure and Nb₂Q $_5$ samples.

Samples	SSA/ m ² .g ⁻¹	(k'/SSA) / 10 ⁻⁵ m' ² -g.min ⁻¹
Nb ₂ O ₅	225.5	1.6
SnO_2	160.0	1.7
Nb ₂ O ₅ / SnO ₂	177.9	4.8

The presence of SnO₂ nanoparticles in the heterostructures resulted in a decrease of SSA, which can be partially explained by the higher SnO₂ density, of around 6.8 g.cm⁻³, and lower specific surface area than Nb₂O₅ (160 m².g⁻¹). However, the heterostructure, even with a lower SSA value than Nb2O5, showed better photocatalytic performance. The process depends on the available surface area of the photocatalyst; thus, k' is called a pseudo-first-order reaction constant. Considering that active sites are constant, as there is no solid dissolution or active site poisoning, this is included in kinetic constant k. Therefore, the k' = k.SSA relationship is valid.^[42] The ratio between k' and SSA indicates the surface area effect in the dye degradation rate, considering it as a reagent in the photocatalytic process, as displayed in Table 1. The data analyses show that the heterostructure's photocatalytic potential per m² is 200 % higher than pure SnO₂ or Nb₂O₅.

Since presumably there is no photocatalyst dissolution, it can be recovered and reused. Thus, Figure 5 shows RhB photocatalytic degradation experiments across five cycles for 180 min. The Nb_2O_5/SnO_2 sample shows a slight drop in efficiency after the first cycle, possibly due to surface saturation. However, it ultimately maintained constant efficiency across the four cycles, proving its reusability in several heterogeneous photocatalytic cycles. Similar result was obtained by Wolski et al. $^{[16]}$, revealing that the reusability of Nb_2O_5 materials is also possible when a Fenton-like process is occurring, showing the versatility of Nb_2O_5 based materials.

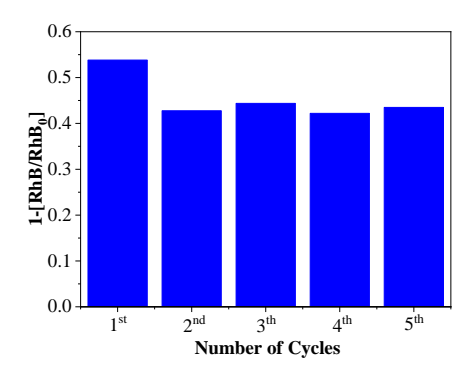


Figure 5. Nb₂O₅/SnO₂ stability during five re-use cycles.

The samples were tested in amiloride degradation (Figure 6), *i.e.*, a drug classified as an emerging contaminant that presents a colorless solution, to check their potential for the degradation of different kinds of organic pollutants.^[27]

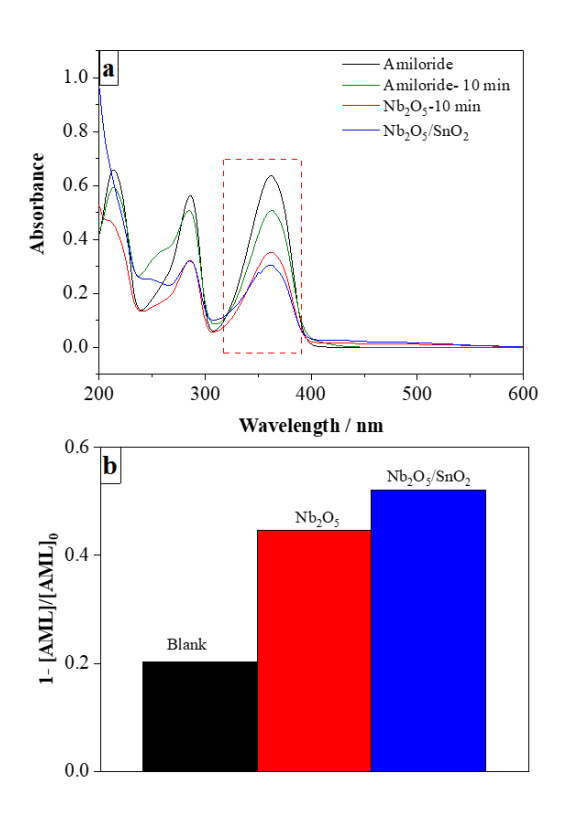


Figure 6. (a) Amiloride absorption spectrum and (b) amiloride degradation percentage after 10 min of UV radiation exposure.

Figure 6(a) shows the amiloride absorption spectrum before and after 10 min of UV exposure. Figure 6(b), meanwhile, shows the amiloride degradation percentage. As presented, about 20% of the amiloride is degraded by light exposure through a direct photolysis process. At the same time, however, all samples were able to promote higher amiloride degradation than direct photolysis, indicating the samples' efficiency. Nb_2O_5/SnO_2 showed better performance than isolated Nb_2O_5 , proving that coupling of the materials improves their photocatalytic potential, even reducing the specific surface area (SSA).

Adsorption performance of the Nb_2O_5 and Nb_2O_5/SnO_2 samples

Figure 7 shows the sample's removal capacity for methylene blue (MB) in the dark and in the presence of UV radiation. Several papers demonstrate that combined adsorption-photocatalysis can improve the photocatalytic performance of semiconductors^[43,44]. Interestingly, both samples presented similar potential. Adsorption played an essential role, as there was no change in the removal rate after UV exposure (the curve's slope did not change). Thus, the primary MB dye removal mechanism is perhaps adsorption over a solid surface. However, the importance of SnO₂ coupling is highlighted, as it produces higher MB adsorption capability per m² of material surface.

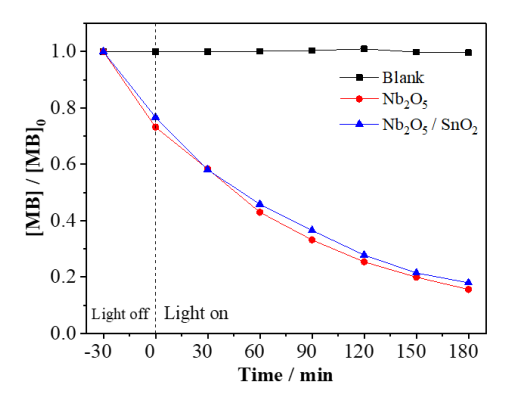


Figure 7. Photodegradation coupled to adsorption under UV light of MB over the as-synthesized samples.

We performed a Zeta potential analysis in order to understand the materials' adsorption capability (Table 2). Both materials exhibit negative surface potential, which plays an essential role in cationic material adsorption. In turn, SnO2 coupling can make the surface even more negative. This effect occurs due to the synthesis method used to obtain the SnO₂ precursor, which results in materials with high negative surface potential.[35] As the synthesized materials presented this important feature with regard to their potential surfaces, they were tested to remove metallic ions, namely Mn(II), in aqueous solution, as can be seen in Table 2. The same pH value of 8.0 was employed during the experiments of Mn (II) adsorption and Zeta potential analysis. The Nb₂O₅/SnO₂ composite material was able to remove around 32% more metal proportion at the same time compared to Nb₂O₅. This effect probably relates to the more negative surface potential due to the SnO₂, increasing the removal performance of cationic compounds in aqueous solution.

Table 1. Zeta Potential and Mn(II) adsorption capability.

Samples	ZetaPotential / (mV)	Mn(II)Adsorption mg _{Mn(II)} /g _{Adsorbent}	1
Nb ₂ O ₅	- 36.0	1.03	
Nb ₂ O ₅ /SnO ₂	- 57.4	1.37	

It is important to note that the adsorption performance was not only related to the surface potential, but also to the specific surface area. Therefore, the Mn (II) adsorption did not increase in the same proportion to surface potential (59 %), since the composites exhibited a lower specific surface area than pure Nb_2O_5 . However, when we compare the adsorption potential per area unit, the composite material presented an increase in adsorption performance of 68 %, close to the increase in the surface potential. Even with the only 1 h of contact, the assynthesized samples presented an adsorption capability comparable to that shown in the literature. [8] This result confirms that Nb_2O_5/SnO_2 composites not only enhanced photocatalytic performance, but also adsorption capacity.

CO₂ Photoreduction

Figure 8 shows the photocatalytic performances for CO_2 conversion in an aqueous system after 6 hours of UV irradiation. Pure Nb_2O_5 shows the capacity to CO_2 conversion into 307 μ mol g^{-1} of CO and a small amount of CH_4 (0.2 μ mol g^{-1}), showing the photocatalytic efficiency of the synthesized material. This relates to the position of its valence and conduction bands, which enables CO_2 activation for C-species formation (CO and CH_4), as well as watersplitting for H_2 evolution. In parallel, the surface contributes, as hydroxyl groups induce distortions in the crystalline network, giving them a negative charge and reducing the interactions between the CO_2/CO and catalyst surfaces. $^{[45]}$ Moreover, the high acidic surface of Nb_2O_5 contributes to increasing interactions with CO_2 molecules. $^{[18]}$

The CO (416 µmol g-1) and H₂ (899 µmol g-1) indicate that the Nb₂O₅/SnO₂ heterostructure is more active for CO₂ reduction (Figure 8). The presence of SnO₂ made the surface of the compound more negative than pure Nb2O5, favoring CO production and earlier CH_4 production.^[18,46] Given the formation of methane, the surface adsorption of CO must occur for subsequent interaction with hydrogen.[47] This justifies a higher production of CO and H₂ and a lower production of CH₄ for the Nb_2O_5/SnO_2 sample than pure Nb_2O_5 . The higher photoactivity of Nb2O5/SnO2 is also seen in its tendency to produce H2. The H2 evolution reaction from water-splitting is the main competitive reaction with CO2 reduction, occurring in lower reduction potentials. However, the mixture between CO and H2 (syngas) with the right ratio is a fuel precursor that is able to create several hydrocarbons and oxygenates, e.g., the synthesis of methanol and ethanol via the Fischer-Tropsch process.[48] This two-step synthetic route, using existing industrial processes, is perceived to be more economicallyviable than the direct conversion of CO2 into multi-electron products, such as methanol or ethylene, as further product separation is highly energy-demanding.^[48,49] Therefore, this is another indication of the better performance of this material for reductive purposes, which can be explored in future research.

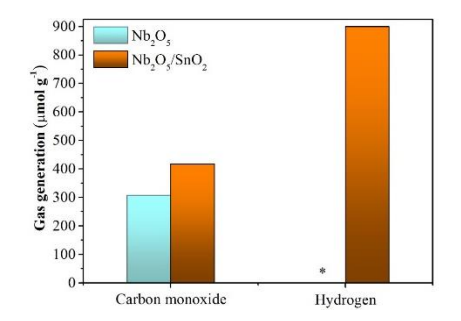


Figure 8. CO₂ photoreduction products and H₂ production using synthesized catalysts activated with UV light after 6 hours. * represents the amount of hydrogen produced by the Nb₂O₅ sample.

In light of the results presented here, we propose a mechanism to explain the formation and higher performance of the Nb₂O₅/SnO₂ heterostructure in environmental treatment compared to isolated Nb₂O₅, as illustrated in Figure 9. First, the Nb₂O₅ crystallization from the niobium peroxo-complex occurs in a reactor environment containing SnO₂ nanoparticles. These nanoparticles attach over the Nb₂O₅ surface without promoting structural changes, as shown in the XRD and Raman analysis. The coupling of small SnO2 nanoparticles, with a diameter of around 5 nm, over Nb2O5 created several points of heterojunction. The photogenerated electrons tend to migrate across the material interface and agglomerate in the SnO2 conduction band due to the Fermi level (E_F) alignment within Nb₂O₅. Positive holes tend to go the other way, agglomerating in the Nb₂O₅ valence band. Once the photogenerated charges reach the materials' surface, due to the increased lifetime, they promote redox reactions as organic molecule degradation or CO₂ reduction. SnO₂ nanoparticles make the Nb₂O₅ surface more negative, as seen in Zeta potential analysis, increasing the interaction with cationic species and making the heterostructured material more efficient for cationic dye or metal removal from water by adsorption.

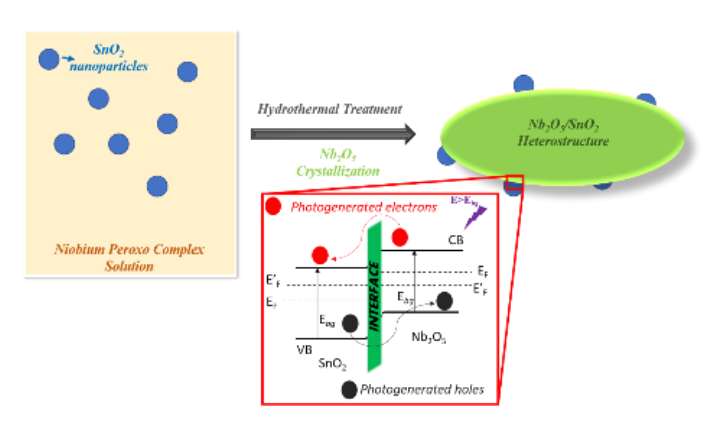


Figure 9. Schematic illustration of the heterostructure formation and photogenerated charge migration.

Conclusion

With the hydrothermal method, Nb_2O_5/SnO_2 heterostructures are promising materials for environmental applications, either for photooxidation or adsorption in the aqueous phase or CO_2 photoreduction. Nb_2O_5/SnO_2 was able to degrade Rhodamine B dye and Amiloride medication under UV radiation and was reused in at least in five cycles. Furthermore, the material can be applied in the removal of cationic species in water, such as methylene blue and Mn(II). Additionally, the material

composition can adjust the product selectivity in CO_2 photoreduction with the aim of producing syngas. These outstanding properties derive from the possible charge migration between oxides following excitation, which increases the photogenerated charges' lifetime and the surface features of the coupled materials. Our results show that the Nb₂O₅/SnO₂ heterostructure is a promising candidate for a single platform with respect to several environmental applications.

Experimental Section

Synthesis

The synthesis of isolated materials was based on previous reports. For Nb₂O₅ preparation, the procedure initially described by Leite et al. and adapted by Lopes et al. $^{[15,33]}$ was used. The synthesis of SnO₂ was based on the procedure reported by Leite et al. $^{[34]}$ The detailed process is described in Sl.

For the synthesis of the composite, preformed SnO₂ was added to the Niobium Peroxo Complex solution prepared as described in SI, in a mass proportion of 1:30 (SnO₂:NH₄H₂[NbO(C₂O₄)₃].*n*H₂O), and have been hydrothermally-treated for 24 h at 150 °C. Then, the resulting material was treated as described for bare Nb₂O₅.

Characterization

The crystalline phases were characterized by X-ray diffraction (XRD) using a Shimadzu XRD-6000 diffractometer. Raman spectroscopy was performed with an FT-Raman spectrometer (Bruker RAM II with a Ge detector). The sample morphology, particle size, and elemental composition were analyzed by scanning electron microscopy (SEM), using a JEOL JEM 2010, which has a Thermo Noran device for measurements of energy-dispersive X-ray spectroscopy (EDS). An FEI Tecnai G2 F20 microscope, operating at 200 kV, was used for the TEM/HRTEM analysis. N₂ adsorption-desorption isotherms were measured with a Micromeritics ASAP 2020 analyzer at 77 K. A Fourier Transform Infrared spectrometer (FTIR) (Bruker VERTEX 70) was then used to investigate the surface features of the samples. UV-vis diffuse reflectance spectroscopy (DRS) was measured in a UV-vis Shimadzu UV-2600 spectrophotometer in diffuse reflectance mode (R). The Tauc plot method was then used to determine the bandgap from DRS spectra[50,51]. The particle surface Zeta potential was analyzed using a Malvern - ZetaSizer model nano-ZS appliance. The characterization procedure's details are shown in the Supplementary Information (SI).

Photocatalysis and Manganese (II) adsorption

The photocatalytic potential of the synthesized samples was evaluated through the degradation of three different contaminants: rhodamine B (RhB) and methylene Blue (MB) dyes, and Amiloride medication, in accordance with previously reported methods[37-39]. All the contaminants solution was used without pH correction. The CO2 photoreduction was performed as outlined in the literature[54]. The reactions were carried out in a liquid medium and the products collected in the headspace. The Mn(II) adsorption was performed as described elsewhere^[8]. In brief, the samples of the materials were added to 15 mL of Mn(II) 2 mg.L-1 solution to obtain a suspension in a concentration of 1 g.L⁻¹, which was continuously stirred. After 1 h, the concentration of Mn(II) was determined with a High-Resolution Continuum Source Atomic Absorption Spectrophotometer (ContrAA ®300, Analytik Jena, Jena, Thuringia, Germany). The results were expressed in mg of Mn(II) adsorbed in 1 g of solid Nb_2O_5 or Nb_2O_5/SnO_2 . The detailed experimental procedure for these steps is described in the SI.

Acknowledgments

The authors are grateful to the São Paulo Research Foundation (FAPESP grant #2017/17553-3 and #2018/01258-5), the National Council for Scientific and Technological

Development (CNPq grant #409904/2016-3, #311463/2017-7, #159866/2018-9 and #407497/2018-8) and IFSP Pro-Rectory of Research. This study was financed in part by the Coordination for the Improvement of Higher Education Personnel - Brazil (CAPES) - Finance Code 001. Brazilian Metallurgy and Mining Company (CBMM) is acknowledged for the Niobium samples supply. OFL would like to thank Alexander von Humboldt Foundation and CAPES by Experienced Research Fellowship (CAPES/Humboldt Agreement - Process 88881.368050/2019-01). The authors thank the Laboratory of Structural Characterization (LCE/DEMa/UFSCar) for the TEM facilities and Lucas Barcelos Otani for TEM/EDS measurements. The authors also gratefully acknowledge Prof. Dr. Tania Regina Giraldi for the laboratory facilities and Thamara M.O. Ruellas for the Mn(II) adsorption measurements.

Keywords: Niobium Oxide; Tin Oxide; Composite; Heterogeneous Photocatalysis: Adsorption.

- K. Nakata, A. Fujishima, J. Photochem. Photobiol. C Photochem Rev 2012, 13, 169–189.
- [2] J. Mao, K. Li, T. Peng, Catal. Sci. Technol. 2013, 3, 2481–2498.
- [3] S. R. Lingampalli, M. M. Ayyub, C. N. R. Rao, ACS Omega 2017, 2, 2740–2748.
- [4] A. L. Linsebigler, G. Lu, J. T. Yates, Chem. Rev. 1995, 95, 735–758.
- [5] C. Chen, W. Ma, J. Zhao, *Chem. Soc. Rev.* **2010**, *39*, 4206–4219.
- [6] V. R. De Mendonça, O. F. Lopes, W. Avansi, R. Arenal, C. Ribeiro, Ceram. Int. 2019, 45, 22998–23006.
- [7] T.R. Giraldi, G. V. F. Santos, V. R. De Mendonca, C. Ribeiro, I. T. Weber, Mater. *Chem. Phys* **2012**, *136*, 505–511. Phys. 136 (2012) 505–511.
- [8] P. Gonçalves, A. F. Barbosa, J. A. de Oliveira, R. Bertholdo, T. R. Giraldi, Int. J. Appl. Ceram. Technol. 2019, 16, 1501–1509.
- [9] A. E. Nogueira, G. T. S. T. da Silva, J. A. Oliveira, J. A. Torres, M.
 G. S. da Silva, M. Carmo, C. Ribeiro, *Catal. Commun.* 2020, 137, 105929.
- [10] X. . He, C. Zhang, J. Mater. Sci. 2019, 54, 8831–8851.
- [11] N. P. de Moraes, F. N. Silva, M. L. C. P. da Silva, T. M. B. Campos, G. P. Thim, L. A. Rodrigues, *Mater. Chem. Phys.* **2018**, *214*, 95– 106.
- [12] A. E. Nogueira, T. C. Ramalho, L. C. A. Oliveira, *Top. Catal.* 2011, 54, 270–276.
- [13] N. T. do Prado, L. C. A. Oliveira, Appl. Catal. B Environ. 2017, 205, 481–488.
- [14] A. M. Raba, J. Barba-Ortega, M. R. Joya, Appl. Phys. A Mater. Sci. Process 2015, 119, 923–928.
- [15] O. F. Lopes, E. C. Paris, C. Ribeiro, Appl. Catal. B Environ. 2014,

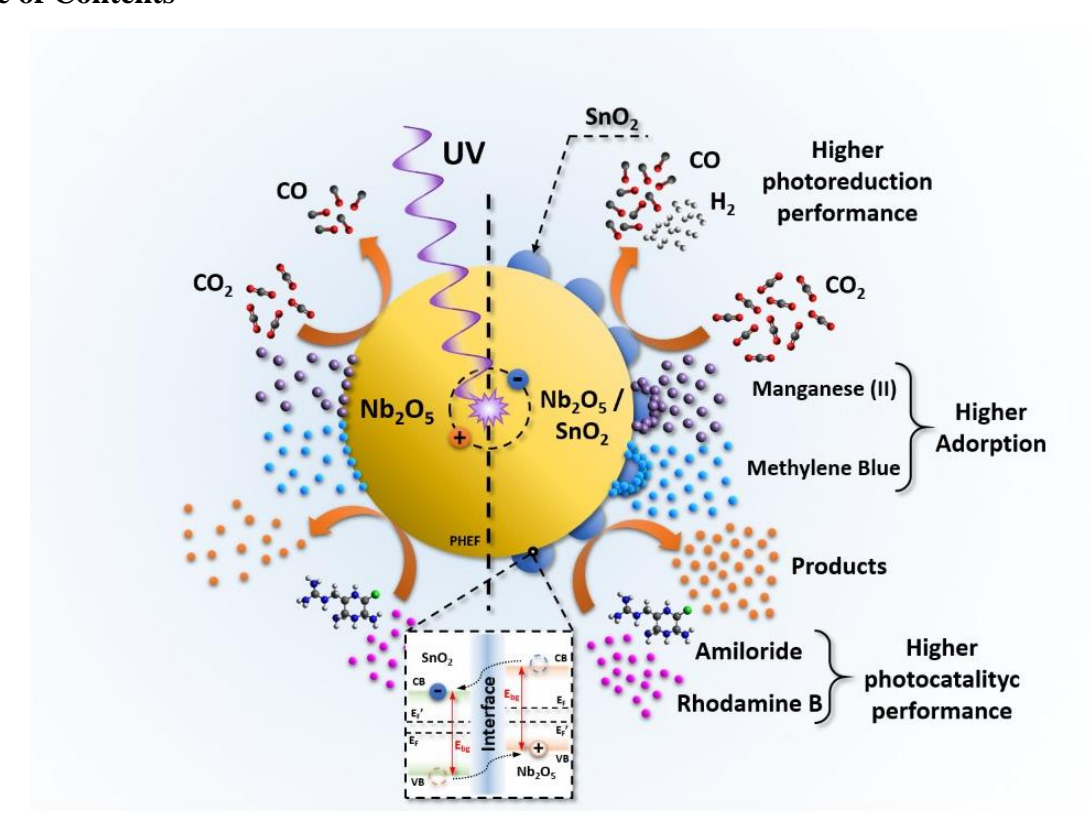
144, 800-808,

- [16] L. Wolski, A. Walkowiak, M. Ziolek, Mater. Res. Bull. 2019, 118.
- [17] E. H. C. Lacerda, F. C. Monteiro, J. R. Kloss, S. T. Fujiwara, J. Photochem. Photobiol. A Chem. 2010. 388. 112084.
- [18] G. T. S. T. da Silva, A. E. Nogueira, J. A. Oliveira, J. A. Torres, O. F. Lopes, C. Ribeiro, Appl. Catal. B Environ. 2019, 242, 349–357.
- [19] F. Nakagomi, S. E. Cerruti, M. R. de Freitas, E. S. Freitas Neto, F. V. de Andrade, G. O. Siqueira, Chem. *Phys. Lett.* **2019**, *729*, 37–41.
- [20] V. R. De Mendonça, O. F. Lopes, A. E. Nogueira, G. T. S. T. da Silva, C. Ribeiro, Nanophotocatalysis and Environmental Applications, Environmental Chemistry for a Sustainable World Vol. 29, (Eds: Inamuddin, G. Sharma, A. Kumar, E. Lichtfouse, A. M. Asiri), Springer, 2019, pp. 107–138.
- [21] V. R. De Mendonça, C. J. Dalmaschio, E. R. Leite, M. Niederberger, C. Ribeiro, J. Mater. Chem. A. 2015, 3, 2216–2225.
- [22] R. T. Bueno, O. F. Lopes, K. T. G. Carvalho, C. Ribeiro, H. A. J. L. Mourão, Quim. Nova. 2019, 42, 661–675.
- [23] N. P. Ferraz, F. C. F. Marcos, A. E. Nogueira, A. S. Martins, M. R. V. Lanza, E.M. Assaf, Y.J.O. Asencios, *Mater. Chem. Phys.* 2017, 198, 131–340.
- [24] J. Yan, G. Wu, N. Guan, L. Li, Appl. Catal. B Environ. 2014, 152– 153, 280–288.
- [25] V. R. De Mendonça, O. F. Lopes, R. P. Fregonesi, T. R. Giraldi,
 C. Ribeiro, Appl. Surf. Sci. 2014, 298, 182–191.
- [26] S. Qianhong, Y. Hui, X. Qiang, Z. Yang, H. Rong, *Mater. Lett.* 2010, 64, 442–444.
- [27] G. T. S. T. da Silva, K. T. G. Carvalho, O. F. Lopes, C. Ribeiro, Appl. Catal. B Environ. 2017, 216, 70–79.
- [28] K. T. G. Carvalho, A. E. Nogueira, O. F. Lopes, G. Byzynski, C. Ribeiro, Ceram. Int. 2017, 43, 3521–3530..
- [29] N. P. Ferraz, A. E. Nogueira, F. C. F. Marcos, V. A. Machado, R.
 R. Rocca, E. M. Assaf, Y. J. O. Asencios, *Rare Met.* 2019, 39, 230–240.
- [30] D. Upadhaya, Talinungsang, P. Kumar, D. D. Purkayastha, Mater. Sci. Semicond. Process. 2019, 95, 28–34.
- [31] X. Q. Qiao, Z. W. Zhang, D. F. Hou, D. S. Li, Y. Liu, Y. Q. Lan, J. Zhang, P. Feng, X. Bu, ACS Sustain. Chem. Eng. 2018, 6, 12375–12384.
- [32] X. Ni, C. Chen, Q. Wang, Z. Li, Chem. Phys. 2019, 525, 110398.
- [33] R. Fiz, F. Hernandez-Ramirez, T. Fischer, L. Lopez-Conesa, S. Estrade, F. Peiro, S. Mathur, J. Phys. Chem. C. 2013, 117, 10086–10094.
- [34] E. R. Leite, E. J. H. Lee, T. R. Giraldi, F. M. Pontes, E. Longo, J.

Nanosci. Nanotechnol. 2004, 4, 774-778.

- [35] C. Ribeiro, E. J. H. Lee, T. R. Giraldi, E. Longo, J. A. Varela, E. R. Leite, J. Phys. Chem. B. 2004, 108, 15612–15617.
- [36] E. R. Leite, C. Vila, J. Bettini, E. Longo, J. Phys. Chem. B. 2006, 110, 18088–18090.
- [37] S. Katayama, Y. Ogawa, H. Hayashi, F. Oba, I. Tanaka, J. Cryst. Growth. 2015, 416, 126–129.
- [38] A. Diéguez, A. Romano-Rodríguez, A. Vilà, J. R. Morante, J. Appl. Phys. 2001, 90, 1550–1557.
- [39] R. F. Brandão, R. L. Quirino, V. M. Mello, A. P. Tavares, A. C. Peres, F. Guinhos, J. C. Rubim, P. A. Z. Suarez, *J. Braz. Chem. Soc.* 2009, 20, 954–966.
- [40] C. M. P. Cecchi, D. Cesarín-Sobrinho, A. B. B. Ferreira, J. C. Netto-Ferreira, Catalysts. 2018, 8.
- [41] V. R. de Mendonça, H. A. J. L. Mourão, A. R. Malagutti, C. Ribeiro, Photochem. Photobiol. 2014, 90, 66–72.
- [42] I. N. Levine, Physical Chemistry, 6th ed., Higher Education, New York, 2009.
- [43] W. Avansi, V. R. De Mendonça, O. F. Lopes, C. Ribeiro, RSC Adv. 2015, 5, 12000–12006.
- [44] S. Kant, D. Pathania, P. Singh, P. Dhiman, A. Kumar, Appl. Catal. B Environ. 2014, 147, 340–352.
- [45] A. K. Kharade, S. Chang, J. Phys. Chem. C. 2020, 124, 10981– 10992.
- [46] G. B. Damas, C. R. Miranda, R. Sgarbi, J. M. Portela, M. R. Camilo, F. H. B. Lima, C. M. Araujo, Catalysts. 2019, 9.
- [47] L. Wang, W. Chen, D. Zhang, Y. Du, R. Amal, S. Qiao, J. Wu, Z. Yin, Chem. Soc. Rev. 2019, 48, 5310–5349.
- [48] F. Urbain, P. Tang, N. M. Carretero, T. Andreu, L. G. Gerling, C. Voz, J. Arbiol, J. R. Morante, Energy Environ. Sci. 2017, 10, 2256–2266.
- [49] W. Sheng, S. Kattel, S. Yao, B. Yan, Z. Liang, C. J. Hawxhurst, Q. Wu, J. G. Chen, Energy Environ. Sci. 2017, 10, 1180–1185.
- [50] J. Tauc, Mater. Res. Bull. 1970, 5, 721–729.
- [51] A. B. Murphy, Sol. Energy Mater. Sol. Cells. 2007, 91, 1326–1337.
- [52] V. R. de Mendonça, C. Ribeiro, Appl. Catal. B Environ. 2011, 105, 298–305.
- [53] K. T. G. Carvalho, O. F. Lopes, D. C. Ferreira, C. Ribeiro, J. Alloys Compd. 2019, 797, 1299–1309.
- [54] J. A. Torres, A. E. Nogueira, G. T. S. T. da Silva, O. F. Lopes, Y. Wang, T. He, C. Ribeiro, J. CO₂ Util. 2020, 35, 106–114.

Table of Contents



- The Nb₂O₅/SnO₂ heterostructure, prepared by means of a facile hydrothermal method, showed higher photocatalytic performance for contaminant degradation, rhodamine B dye and amiloride medicine, and CO₂ photoreduction, producing syngas. Besides, cationic species adsorption was higher over the heterostructure than isolated Nb₂O₅, showing the versatility of the as prepared heterostructured composite.